Large Magnetoresistance in Few Layer Graphene Stacks with Current Perpendicular to Plane Geometry

Zhi-Min Liao, Han-Chun Wu,* Shishir Kumar, Georg S. Duesberg, Yang-Bo Zhou, Graham L. W. Cross, Igor V. Shvets, and Da-Peng Yu*

Magnetoresistive structures have promising applications in magnetic random access memory and magnetic sensors. Ferromagnetic granular alloys display an anisotropic magnetoresistance (MR) effect;[1] spin valves based on magnetic multilayers exhibit giant MR;[2,3] manganite perovskites demonstrate colossal MR resulting from magnetic field induced metal-insulator transition;[4,5] magnetic tunnel junctions consisting of a thin nonmagnetic insulator sandwiched by two ferromagnetic layers present a tunnelling MR effect;[6,7] other materials including single-crystal bismuth thin films,[8] silver chalcogenides[9] and indium antimonide[10] have a large MR effect.

Graphene is a single-atom-thick sheet with an hexagonal arrangement of carbon atoms that results in its massless fermion, high carrier mobility, and linear dispersion relation.[11–14] Investigations on magnetoresistance (MR) of graphene not only provide an effective method to explore the electron transport properties but also open a suitable window for magnetoelectronic applications.[15–19] Recently, a spin-filter design was proposed consisting of graphene sandwiched between two layers of ferromagnetic material.[20] For this purpose, graphene based spin-valves were fabricated using ferromagnetic (FM) metal[21] or FM metal oxide[22] electrodes. Around 20% MR was predicted theoretically due to the strong interaction between graphene and the Ni layer[23] and 4% MR was found experimentally at room temperature due to the existence of a tunnel barrier at the interface between graphene and the FM metal oxide layer.[22] Apart from the graphene/FM interface, the electron transport through graphene in the current-perpendicular-to-plane (CPP) configuration is also crucial to graphene MR devices. Here, we report a large MR effect up to 100% at low temperatures and over 60% at room temperature under magnetic field of 14 T of few layers graphene stacks sandwiched by two non-magnetic metal electrodes in the CPP configuration. The MR exhibits a strong anisotropy depending on the angle between the direction of the magnetic field and the graphene plane. Moreover, the resistance of the device is only tens of ohms in the two-probe configuration which can be further reduced for four-probe measurements, having the advantage of low power consumption for magnetic device applications.

In this study large-area graphene, with a typical dimension of 1 cm × 1 cm grown on Cu foil, was transferred onto a SiO_2 substrate covered with a 200 nm thick Cu film using the wet-etching method. The graphene stacks were obtained by superposing the monolayer graphene with a random orientation using the transfer-printing technique.[24] The Raman spectrums of the graphene stacks are shown in Figure S1 in Supporting Information, which indicate the random orientation between graphene layers fabricated by the layer-by-layer transfer-printing method. A sketch of the graphene MR device in this study is shown in **Figure 1**(a) where the bias is applied perpendicular to the graphene plane. The bottom Cu film served as one of the electrodes, and the top electrode was fabricated at the centre of the graphene layer by directly gluing a gold wire onto the graphene surface using silver epoxy with a typical contact area ~100 × 100 μm^2. The magnetic field (H) dependent resistance (R) as the charge carriers vertically transported through two monolayers of graphene is shown in Figure 1b,c. Remarkably, for the magnetic field perpendicular to the graphene plane ($\theta = 0°$), a large positive magnetoresistance (MR) up to ~100% with no sign of saturation was observed at 14 T as shown in Figure 1(b). Here, the MR is defined as MR=R(H)/R(0)-1, and the angle θ is the angle between the direction of the magnetic field and the normal direction of the graphene plane. Moreover, one can see from Figure 1(b) that the MR exhibits a strong dependence on θ. At 14 T, the MR gradually decreased from 100% to 2% as the sample plane is rotated from perpendicular ($\theta = 0°$) to parallel ($\theta = 90°$) to the magnetic field. At low magnetic fields (see Supporting Information Figure S2(a)), there is a negative MR which usually results from a weak localization effect. The magnetic field values for the minimum MR increase from 0.3 T to ~2.5 T as θ is changed from 0° to 90°. Figure 1(c) shows the MR at different temperatures in the perpendicular magnetic field configuration. One can see that the large positive MR is rather robust and its value is over 60% at 14 T and at 300 K. The weak localization effect at low magnetic field reduces with increasing temperature and disappears above 50 K, as shown in Figure S2(b).

Prof. Z.-M. Liao,[+] Y.-B. Zhou, Prof. D.-P. Yu
State Key Laboratory for Mesoscopic Physics
Department of Physics
Peking University
Beijing 100871, P.R. China
E-mail: liaozm@pku.edu.cn
Dr. Z.-M. Liao, Dr. H.-C. Wu,[+] Prof. G. L. W. Cross, Prof. I. V. Shvets
Centre for Research on Adaptive Nanostructures and Nanodevices (CRANN)
and School of Physics
Trinity College, Dublin 2, Ireland
E-mail: wuhc@tcd.ie
S. Kumar, Prof. G. S. Duesberg
Centre for Research on Adaptive Nanostructures and Nanodevices (CRANN)
and School of Chemistry
Trinity College, Dublin 2, Ireland
[+] Z.M.L. and H.C.W. contributed equally to this work.

DOI: 10.1002/adma.201104796

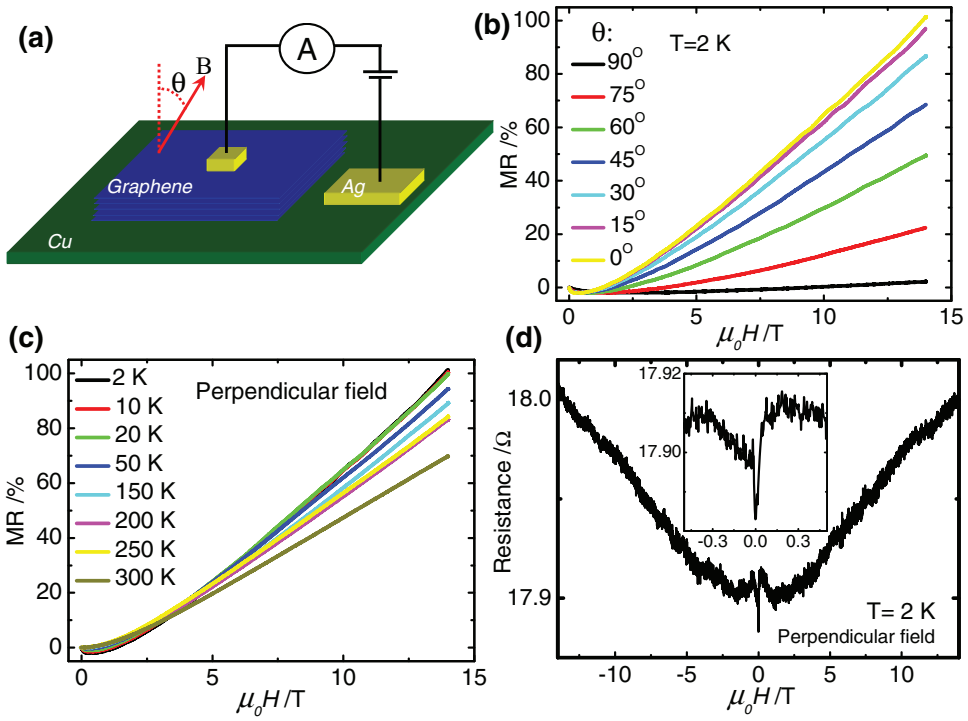

Figure 1. Magnetoresistance of the graphene stack via vertical transport measurements. (a) Schematic of a graphene stack sandwiched by two electrodes. The graphene grown on Cu foil by CVD method was transferred layer-by-layer to form the graphene stack. (b, c) The MR of a two-layer graphene stack, (b) measured at 2 K with different angles between the normal of the graphene plane and the magnetic field, and (c) measured with perpendicular fields at different temperatures. (d) The MR of only a monolayer graphene. Inset: the MR at low field shows the weak antilocalization effect.

Generally, graphene is considered as a non-magnetic material. Although graphene can be magnetized through formatting zigzag edges and generating artificial point defects,[25] we believe that our studied pristine graphene samples should be of nonmagnetic nature without any additional treatments. Therefore, it is surprising that the electron tunneling through the nonmagnetic two-layer graphene stack can result in such a large MR. To rule out the possible contributions due to the graphene/metal interfaces, we fabricated Ag/graphene/Cu sandwiched MR devices with only a single monolayer of graphene using the same process. The MR for monolayer graphene is shown in Figure 1(d). For the magnetic field perpendicular to the graphene plane ($\theta = 0°$), only a small MR ~ 0.66% at 14 T was observed. Nevertheless, the weak anti-localization effect is still clearly observed at low magnetic field (inset in Figure 1(d)), which indicates the MR effect is from the single layer graphene.[26] Therefore, the observed large MR effect being due to the graphene/metal interfaces can be ruled out. First, the MR is very low for the single layer graphene MR device which has similar graphene/metal interfaces, while we observed a large MR effect over 100% for the graphene stacks. Secondly, a weak anti-localization effect was observed at low magnetic fields for the single layer graphene while the graphene stacks present a weak localization effect. For the randomly stacked two-layer graphene, the suppression of weak anti-localization and appearance of negative MR originating from weak localization are due to the carriers transport through the phase-coherent disordered graphene.[26]

We believe that this large positive MR in the two-layer graphene stack originates from the graphene/graphene interface when carriers transport vertically through the two-layer graphene. As the graphene stack was obtained by superposing the monolayer graphene with random orientation, the carbon atoms of the top layer will not lie exactly on the top of the carbon atoms in the bottom layer. Under an external electrical field, carriers will change their direction to find the nearest neighbor carbon atoms in the bottom layer, which will result in an in-plane velocity. Furthermore, boundaries, defects and impurities may be introduced to the interface during the transfer-printing process. The introduced boundaries, defects and impurities will work as the scattering centers and reduce the mobility. The carriers will be scattered at the graphene/graphene interface before they tunnel into the Cu layer which is supported by the appearance of the weak localization effect at low magnetic field. In addition to the above mentioned mechanisms of in-plane velocity, there are some other factors that can also give rise to positive MR. Under a magnetic field perpendicular to the graphene plane, Zeeman splitting and Coulomb interaction between electrons will lift the valley and orbital degeneracy of the zero-energy Landau Level which also result in an increase of the resistance.[27]

As the carriers have an in-plane velocity when they are transported vertically through the two-layer graphene stack, we would like to outline below a quantitative description of its contribution to the observed MR. Usually, there are two other main contributions to the graphene MR effect apart

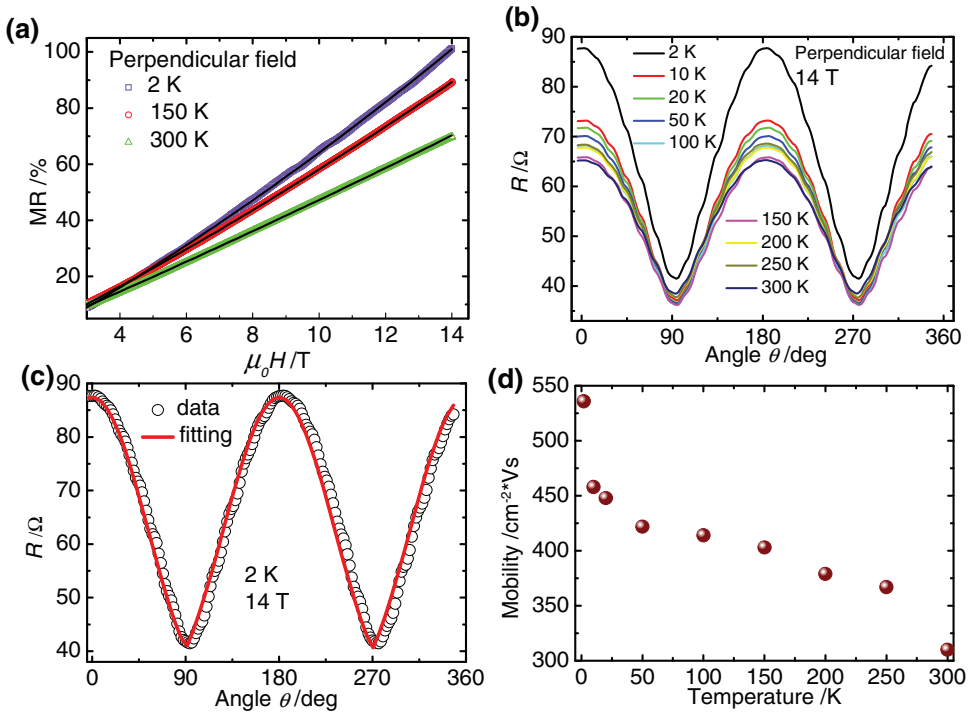

Figure 2. Temperature and angle θ dependence of MR of a two-layer graphene stack. (a) The MR data at magnetic field higher than 3 T were fitted well by considering both linear and quadratic dependence. (b) Resistance as a function of angle θ at a fixed magnetic field of 14 Teslas and different temperatures. (c) A typical fitting result (the solid line) for the R(θ) data (the open circles) measured at B = 14 T and T = 2 K by considering the vertical component of the magnetic field. (d) Mobility as a function of temperature obtained from the fitting of the data in (b).

from the weak (anti-)localization effect. The first is due to the curving of electron trajectories in the graphene plane which usually results in a positive MR with a quadratic magnetic field dependence MR $\propto (\mu H)^2$, where μ is the carrier mobility.[28] Another one is the so-called linear MR, which has been observed in many systems, such as in multi-layer graphene[15] and doped Ag_xSe.[9] The linear MR has two possible descriptions: quantum linear MR and classical linear MR. Abrikosov proposed a quantum description for a zero band gap system to explain the linear MR behavior.[29] The conditions for the quantum linear MR are $\omega_c \gg K_BT$ and $n \ll (eH/c)^{3/2}$, where T is temperature and n is carrier concentration. Parish and Littlewood (PL) proposed an alternative classical description to this linear MR.[30] They proposed that the gross inhomogeneity in a 2D-random resistor network can produce distorted current paths misaligned with the bias direction, contributing to the off-diagonal components in the resistivity tensor. Because the system inhomogenous is favorable for the appearance of the large positive MR, we believe that the MR will decrease if the two graphene layers have the same orientation.

Figures 1(b,c) show that the MR deviates from the linear relationship and displays super-linear dependence. In our MR devices, the carrier mobility μ may be very low due to the existence of boundaries, defects and impurities. Therefore, the classical MR with quadratic dependence with H cannot be neglected at $\mu(\mu_0 H) < 1$, where μ_0 is the vacuum permeability. The experimentally observed MR can be quantitatively given as

$$MR = R(H)/R(0) - 1 = p \times H + (\mu\mu_0 H)^2 \quad (1)$$

where p is the proportional coefficient. All the experimental data presented in Figures 1(b,c) can be well fitted by Equation (1), and the typical fitting results were summarized in **Figure 2**(a). At a perpendicular magnetic field of 14 T, the resistance was measured as a function of θ for different temperatures, as shown in Figure 2(b). The experimental data R(θ) can be fitted well by considering the vertical component of the magnetic field and can be formulated as

$$\begin{aligned} R(14T,\theta) &= R(0)\left[1 + p \times H_\perp + (\mu\mu_0 H_\perp)^2\right] \\ &= R(0)\left[1 + (p/\mu_0) \times (14T) \times |\cos\theta|\right] \\ &+ R(0)\left[(\mu \times (14T) \times \cos\theta)^2\right] \end{aligned} \quad (2)$$

where the carrier mobility μ is related to the carriers transport through the device and contains the combined effects of both perpendicular and in-plane transport paths. All of the data of R(θ) presented in Figure 2(b) can be well fitted by Equation (2), and a typical fitting result for T = 2 K is shown in Figure 2(c). As a parameter, the carrier mobility μ is obtained from the curve fitting, and the values at different temperatures are presented in Figure 2(d). The calculated carrier mobility is ~536 cm^{-2} V·s at 2 K, and the criterion $\mu(\mu_0 H) < 1$ is satisfied for the quadratic MR dependence for our experimental conditions. The carrier mobility decreases with increasing temperature. As a consequence, the quadratic term of the MR will be

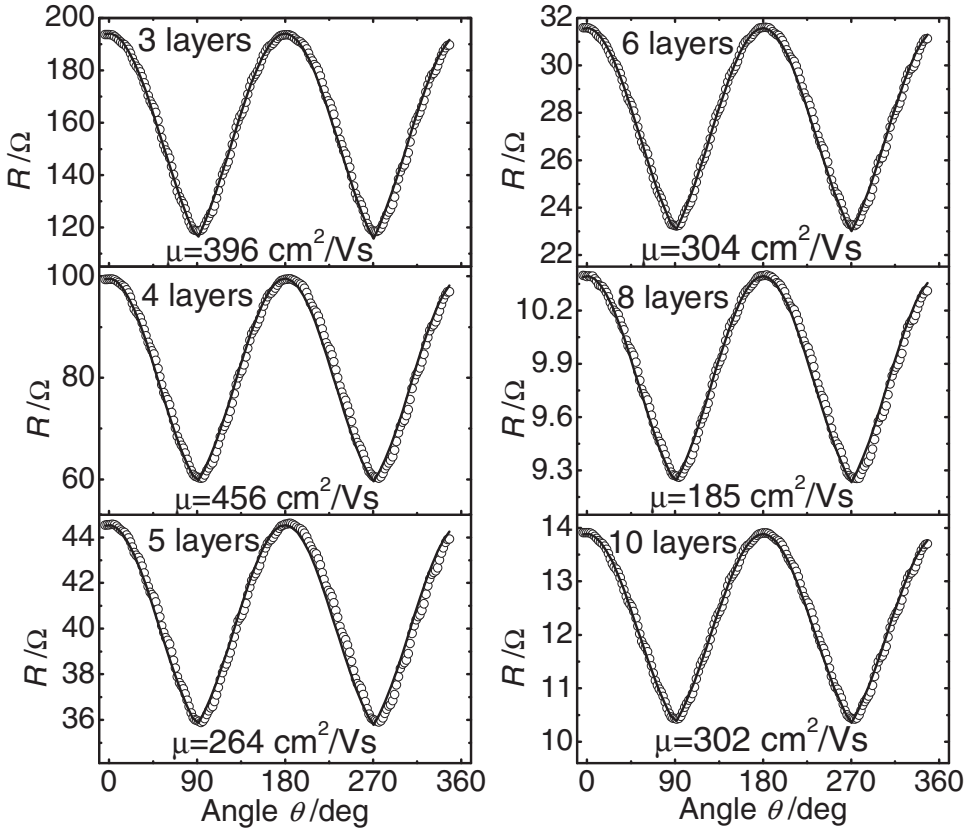

Figure 3. Layer dependence of MR of graphene stacks. The resistance plotted against the angle θ of the graphene stack with different layers at temperature of 10 K and magnetic field of 14 T. The data of R(θ) are well fitted (the solid lines) and the calculated mobilities are denoted.

less notable and the MR is closer to a linear dependence with H at higher temperature, which is consistent with the data in Figure 1(c).

To demonstrate that the MR effect observed in two-layer graphene is a general effect for a graphene stack, Supporting Information Figure S3 shows the MR of the graphene stack with different number of graphene layers measured at 10 K and with perpendicular magnetic fields. It is found that all the graphene stacks show a large positive MR effect. However the exact MR ratio and resistance vary from sample to sample and do not have a regular dependence on the number of layers. To reveal the underlying physics of the observed MR behaviors, the data of R(θ) at 14 T and a temperature of 10 K for samples with different numbers of graphene layers are presented in **Figure 3**. The data of R(θ) are well fitted by Equation (2), and the mobilities calculated from the fitting results are denoted in Figure 3. Interestingly, we found that the MR ratio depends crucially on carrier mobility. The MR value (at 14 T) as a function of mobility is shown in **Figure 4**. The higher the mobility is, the larger the MR magnitude will be. The carrier mobility may be susceptible to the transfer-printing process and may vary from sample to sample, and thus the MR values vary from sample to sample.

To further reveal the transport properties of the graphene stack with CPP configuration, some detailed analyses and experiments were performed. First, from the data presented in Figure 1(b), the MR oscillations at 2 K were observed by subtracting the positive MR background, as shown in Figure S4. As the sample plane was rotated from the $\theta = 0°$ (perpendicular magnetic field) to $\theta = 15°$, 30°, the oscillation patterns move to higher magnetic fields with $H(\theta) = H_{\perp}/\cos\theta$. We believe that the MR oscillations superimposed on the large positive MR background may originate from the two-dimensional nature of graphene. Second, the

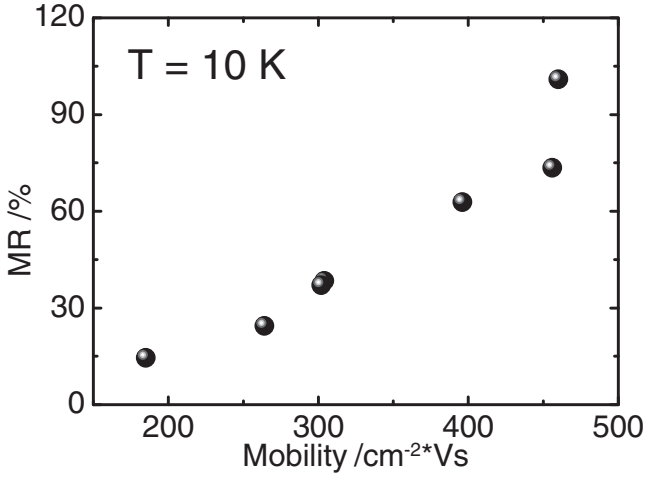

Figure 4. The data of carrier mobility vs. magnetoresistance at 14 T collected from Figure 3 for the graphene stacks with different numbers of layers.

device with the graphene area defined as the same of the top contact was fabricated. The schematic device structure is shown in Figure S5(a). After fabricating the top contact, the uncovered graphene was etched away by plasmas using the top contact as a hard mask. The MR of this structure with a four-layer graphene stack is shown in Figure S5(b), and the very similar large positive MR were obtained under perpendicular magnetic field. Third, the effect of dc current on the MR was also studied. We have measured the current-voltage (I–V) curves of a ten-layer graphene stack under zero and 14 T magnetic field, as shown in Figure S6. From the linear I–V curves we can obtained the MR(14 T) = R(14 T)/R(0)-1 is independent with the current bias.

In conclusion, we have fabricated layer-controllable graphene stacks. Large magnetoresistance up to 100% at 14 T was observed as the carriers transport vertically through two-layer graphene stack, and the whole device has very low resistance of several tens of ohms. The MR was strongly dependent on the angle between the graphene plane and the direction of the magnetic field. The ultra-thin graphene cell may have potential applications in electronics and magnetic devices.

Experimental Section

Device fabrication: The graphene was grown on copper foil by a chemical vapor deposition method using CH_4 and H_2 as precursor gases. Then, Poly(methyl methacrylate) (PMMA) was coated on the graphene and the copper foil was dissolved by wet chemical etching. The PMMA/graphene thin film was then processed by thermal tape and put down on a SiO_2 substrate with a 200 nm thick Cu film. After releasing the thermal tape and dissolving the PMMA, a single layer graphene was laid on the substrate. Trough layer-by-layer printing the graphene on the substrate, a multi-layer graphene stack was formed.

Measurements: The electron transport properties of the graphene devices were measured using Keithley 2400 source-meter units. Constant dc current of 100 μA was used for MR measurements. The magnetic field and temperature were well controlled using a physical properties measurement system (PPMS-14 T, Quantum Design). The sample holder can rotated to tune the angle between the sample plane and direction of the magnetic field. The Raman spectrums of the graphene were characterized by a Renishaw invia Raman optical system using a laser with wavelength of 514 nm as excitation.

Supporting Information

Supporting Information is available from the Wiley Online Library or from the author.

Acknowledgements

This work was supported by NSFC (No. 10804002), MOST (Nos. 2012CB933401, 2009CB623703), the Sino Swiss Science and Technology Cooperation Program (2010DFA01810), and Science Foundation of Ireland Grants No. 06/IN.1/I91, 008/IN.1/I1932, and 08/CE/I1432. We are grateful to Prof. Q.F. Sun and Prof. X.C. Xie at PKU for inspired discussions.

Received: December 15, 2011
Revised: February 1, 2012
Published online: March 7, 2012

[1] T. McGuire, R. Potter, *IEEE Trans. Magn.* **1975**, *11*, 1018.
[2] P. Grünberg, R. Schreiber, Y. Pang, M. B. Brodsky, *Phys. Rev. Lett.* **1986**, *57*, 2442.
[3] M. N. Baibich, J. M. Broto, A. Fert, F. Nguyen Van Dau, F. Petroff, P. Eitenne, G. Creuzet, A. Friederich, J. Chazelas, *Phys. Rev. Lett.* **1988**, *61*, 2472.
[4] R. von Helmolt, J. Wecker, B. Holzapfel, L. Schultz, K. Samwer, *Phys. Rev. Lett.* **1993**, *71*, 2331.
[5] S. Jin, T. H. Tiefel, M. McCormack, R. A. Fastnacht, R. Ramesh, L. H. Chen, *Science* **1994**, *264*, 413.
[6] T. Miyazaki, N. Tezuka, *J. Magn. Magn. Mater.* **1995**, *139*, L231.
[7] S. S. P. Parkin, C. Kaiser, A. Panchula, P. M. Rice, B. Hughes, M. Samant, S. H. Yang, *Nat. Mater.* **2004**, *3*, 862.
[8] F. Y. Yang, K. Liu, K. Hong, D. H. Reich, P. C. Searson, C. L. Chien, *Science* **1999**, *284*, 1335.
[9] R. Xu, A. Husmann, T. F. Rosenbaum, M.-L. Saboungi, J. E. Enderby, P. B. Littlewood, *Nature* **1997**, *390*, 57.
[10] J. Hu, T. F. Rosenbaum, *Nat. Mater.* **2008**, *7*, 697.
[11] K. S. Novoselov, A. K. Geim, S. V. Morozov, D. Jiang, M. I. Katsnelson, I. V. Grigorieva, S. V. Dubonos, A. A. Firsov, *Nature* **2005**, *438*, 197.
[12] Y. Zhang, Y. W. Tan, H. L. Stormer, P. Kim, *Nature* **2005**, *438*, 201.
[13] D. L. Miller, K. D. Kubista, G. M. Rutter, M. Ruan, W. A. de Heer, P. N. First, J. A. Stroscio, *Science* **2009**, *324*, 924.
[14] A. Bostwick, F. Speck, T. Seyller, K. Horn, M. Polini, R. Asgari, A. H. MacDonald, E. Rotenberg, *Science* **2010**, *328*, 999.
[15] A. L. Friedman, J. L. Tedesco, P. M. Campbell, J. C. Culbertson, E. Aifer, F. K. Perkins, R. L. Myers-Ward, J. K. Hite, C. R. Eddy Jr., G. G. Jernigan, D. K. Gaskill, *Nano Lett.* **2010**, *10*, 3962.
[16] W. Y. Kim, K. S. Kim, *Nat. Nanotechnol.* **2008**, *3*, 408.
[17] F. Munoz-Rojas, J. Fernandez-Rossier, J. J. Palacios, *Phys. Rev. Lett.* **2009**, *102*, 136810.
[18] J. W. Bai, R. Cheng, F. X. Xiu, L. Liao, M. S. Wang, A. Shailos, K. L. Wang, Y. Huang, X. F. Duan, *Nat. Nanotechnol.* **2010**, *5*, 655.
[19] J. M. Lu, H. J. Zhang, W. Shi, Z. Wang, Y. Zheng, T. Zhang, N. Wang, Z. K. Tang, P. Sheng, *Nano Lett.* **2011**, *11*, 2973.
[20] V. M. Karpan, G. Giovannetti, P. A. Khomyakov, M. Talanana, A. A. Starikov, M. Zwierzycki, J. van den Brink, G. Brocks, P. J. Kelly, *Phys. Rev. Lett.* **2007**, *99*, 176602.
[21] S. Cho, Y.-F. Chen, M. S. Fuhrer, *Appl. Phys. Lett.* **2007**, *91*, 123105.
[22] Z. M. Liao, H. C. Wu, J. J. Wang, G. L.W. Cross, S. Kumar, I. V. Shvets, G. S. Duesberg, *Appl. Phys. Lett.* **2011**, *98*, 052511.
[23] V. M. Karpan, G. Giovannetti, P. A. Khomyakov, M. Talanana, A. A. Starikov, M. Zwierzycki, J. van den Brink, G. Brocks, P. J. Kelly, *Phys. Rev. Lett.* **2007**, *99*, 176602.
[24] Y.-Q. Bie, Y.-B. Zhou, Z.-M. Liao, K. Yan, S. Liu, Q. Zhao, S. Kumar, H. C. Wu, G. S. Duesberg, G. L.W. Cross, J. Xu, H. L. Peng, Z. F. Liu, D. P. Yu, *Adv. Mater.* **2011**, *23*, 3938.
[25] R. R. Nair, M. Sepioni, I-Ling Tsai, O. Lehtinen, J. Keinonen, A. V. Krasheninnikov, T. Thomson, A. K. Geim, I. V. Grigorieva, *Nat. Phys.* **2012**, doi:10.1038/nphys2183.
[26] E. McCann, K. Kechedzhi, I. Vladimir Fal'ko, H. Suzuura, T. Ando, B. L. Altshuler, *Phys. Rev. Lett.* **2006**, *97*, 146805.
[27] Y. Zhao, P. Cadden-Zimansky, Z. Jiang, P. Kim, *Phys. Rev. Lett.* **2010**, *104*, 066801.
[28] J. L. Olsen, *Electron Transport in Metals*, Interscience, New York **1962**.
[29] A. A. Abrikosov, *Europhys. Lett.* **2000**, *49*, 789.
[30] M. M. Parish, P. B. Littlewood, *Nature* **2003**, *426*, 162.